

Image Restoration

Carsten Denker

*New Jersey Institute of Technology, Center for Solar-Terrestrial Research,
Newark, New Jersey, U.S.A.*

Alexandra Tritschler

*New Jersey Institute of Technology, Big Bear Solar Observatory,
Big Bear City, California, U.S.A.*

Mats Löfdahl

*Royal Swedish Academy of Sciences, Institute for Solar Physics, AlbaNova University Center,
Stockholm, Sweden*

INTRODUCTION

Throughout the past two decades, digital image processing has made its way into today's technology and computer driven society. Its applications encompass a wide variety of specialized disciplines including medical imaging, machine vision, remote sensing, and astronomy—even influencing the computer user at home. Personal images obtained with digital cameras can easily be manipulated by a variety of dedicated commercial and public domain image processing software packages. Image restoration has to be defined in this context. Whereas image enhancement strives to bring out certain features in an image to simplify the extraction of image information, image restoration is the attempt to retrieve information that has been lost or obscured in the imaging process itself, thus, obtaining a result that is closer to an ideal image of the object. Therefore, image restoration requires a systems approach that takes into account the entire process of image formation including the propagation of light through inhomogeneous media, the properties of the optical system, and the characteristics of the detector. Here, solar astronomy will serve as an example of the image formation process. We will discuss various image restoration methods and the underlying mathematical models.

BACKGROUND

Images are nowadays obtained in spectral regions across the entire electromagnetic spectrum:^[1] Positron emission tomography (PET) is used in γ -ray nuclear imaging to identify infections or tumors in bones. The Chandra X-ray observatory is surveying high-energy regions of the universe. Fluorescence microscopy in the ultraviolet has a wide range of

applications in biomedical imaging. Examples of imaging in infrared and visible bands are too numerous to count and include astronomy, remote sensing, machine vision, microscopy, etc. The most common application of microwave imaging is radio detection and ranging (RADAR). Finally, radio waves are used in magnetic resonance imaging (MRI) and large arrays of radio antennas utilize aperture synthesis in radio astronomy to yield high-spatial resolution images of astronomical objects. However, digital images are not only recorded in the electromagnetic spectrum. Sound or pressure waves are used to probe geological formations and ultrasound imaging provides an unobtrusive means to glean inside the human body. Because of the particle-wave duality, particle beams can also form images. Examples include transmission electron microscopy (TEM) and scanning electron microscopy (SEM). Digital images are currently replacing their photographic counterparts. For example, this transition process has already been concluded in astronomy but is still underway in medical imaging. This transition is accelerated by the exponential increase of computing power, data storage, and network bandwidth, commonly known as Moore's law. Therefore, data mining, pattern recognition, feature extraction, and data visualization are frontier research areas with broad impacts on our technology driven society. The topic of "Image Restoration" is covered in many introductory textbooks specializing in digital image processing, computer vision, and image and signal processing.^[1–4] The current research efforts in these scientific disciplines can be followed in many refereed journals and conference proceedings.^[5–8]

Image restoration encompasses the entire image formation process and provides a foundation for the subsequent steps of image processing. The goal is to retrieve image information that has been corrupted in the process of image formation. In contrast to image

enhancement, where the appearance of an image is improved to suit some subjective criteria, image restoration is an objective approach to recover a degraded image based on mathematical and statistical models. In a first step, we have to characterize the object of our observation, which could be a faint point source (e.g., a single star in the nighttime sky) or a bright extended object such as the Sun. Some of the image degradation is usually attributed to the propagation of the wave or particles through an inhomogeneous medium. To identify retinal diseases in the posterior of our eye, we have to observe through the turbid vitreous liquid in our eyes and in the case of ground-based astronomical observations, the Earth's turbulent atmosphere will degrade and blur images.^[9] Obviously, by obtaining images from space we can alleviate these complications in the astronomical image formation process. However, this can be costly and add to technological complexity. In medical applications, the simplistic approach of removing the inhomogeneous medium might not even be feasible. Adaptive optics^[10,11] is an approach to correct wavefront phase aberrations in real-time. Here, information of the atmospheric turbulence is extracted from images in real-time and transferred to a deformable mirror to minimize image degradation in a feed-back loop. The next step of the image formation process has to address the instrument itself. For example, the central obscuration of a Cassegrain telescope changes the image contrasts compared to unobscured telescopes. Finally, we have to study the characteristics of the image detector and its noise characteristics. Modern charge coupled device (CCD) and complex metal-oxide semiconductor (CMOS) detectors detect up to 90% of the incident photons. The noise is given by the photon statistics and the read-out circuitry of the detectors. In the following sections, we will describe some of the image restoration techniques that are currently employed in astronomical and solar observations. However, similar techniques are used in many other areas of image restoration and our choice of astronomical techniques only reflects our professional bias.

IMAGE RESTORATION

The light originating from stars, planets, or our Sun starts out as a spherical wavefront. However, considering the enormous distances between celestial objects, we can assume that the light enters the Earth's turbulent atmosphere as a plane parallel wavefront. Wavefront aberrations, i.e., deviations from a planar geometry, could arise from atmospheric turbulence or imperfect optics. The day-night cycle is responsible for heating and cooling the Earth's surface creating large-scale atmospheric motions. Once these motions

become turbulent, large-scale eddies break up into smaller and smaller eddies leading to temperature fluctuations across a wide range of spatial scales. Since the refractive index of air is temperature sensitive, atmospheric turbulence will change the path and thereby the amplitude and phase of the light that falls onto the telescope aperture, and thereby limits the effective resolution of a long-exposure image. The energy transfer from large- to small-scale turbulent eddies is governed by Kolmogorov's model of atmospheric turbulence, which derives spatial power spectra for fluctuations of the refractive index.^[10] Short-exposure images retain diffraction-limited information by "freezing" the wavefront aberrations.^[12] The typical correlation time-scale for daytime observations is about 10ms and can increase to more than 100ms under excellent nighttime observing conditions. Astronomers summarize the effects of atmospheric turbulence in the expression "seeing," which includes image motion, differential image motion or distortions, and blurring. The basis of many image restoration methods is therefore a set of short-exposure data frames with the same object but different realizations of wavefront aberrations. Dynamic processes, such as the ever changing surface of the Sun, would violate the underlying assumption of an unaltered object. Thus, the time to collect images containing sufficient statistical information on atmospheric turbulence can be short (less than a minute for solar observations).

The diffraction pattern or point-spread function (PSF) of an aberration-free instrument with circular aperture consists of a central bright region, the "Airy disk," and several fainter rings separated by circles of zero intensity (see Fig. 1 for a one-dimensional cross-section of the Airy function). The intensity distribution of a pointlike object is given by

$$d(x) = d_0 \left(\frac{2J_1(x)}{x} \right)^2 \quad (1)$$

where d_0 is the peak intensity of the Airy disk and $J_1(x)$ is a Bessel function of the first kind of order unity

$$J_1(x) = x \sum_{n=1}^{\infty} (-1)^{n+1} \frac{x^{2n-2}}{(n-1)!n!2^{2n-1}} \quad (2)$$

The argument of the intensity distribution is $x = (\pi D/\lambda)\sin\theta$, where λ is the wavelength, D is the diameter of the aperture, and θ is the angular distance from the pattern maximum. In general, the PSF of a system has to include the phase of the aperture function of the optical instrument describing the effects of atmospheric turbulence. The optical transfer function (OTF) is the Fourier transform of

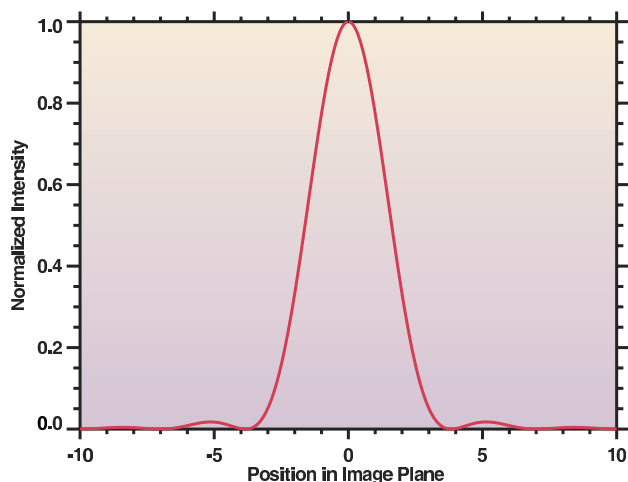


Fig. 1 Airy function. The Airy function describes the (one-dimensional) diffraction pattern of a point source observed through an instrument with a circular entrance aperture. (View this art in color at www.dekker.com.)

the PSF and describes how the system transfers the spatial frequency contents of an object. The OTF by itself is a measure of the quality of the imaging system. The modulus of the OTF is the modulation transfer function (MTF) describing the imaging system's modulation of the spatial frequency contents of the object. In other words, the MTF describes the ability of an optical system to transfer spatial details. In Fig. 2, we compare the MTFs of imaging systems with circular, donut-shaped, and square apertures. The collecting area of the aperture functions were chosen such that the MTFs approach zero at the same normalized spatial frequency. Therefore, the photon flux and thus the sensitivity of the instruments will be different. This leads to the question, how to define the spatial resolution of an optical system, i.e., what is the smallest detail that can be reliably recovered?

The answer is summarized in the Rayleigh criterion." If two point sources are sufficiently close together, the diffraction patterns begin to overlap and become at some point indistinguishable. Since there is no sharp boundary between two overlapping intensity distributions, resolution criteria are by nature somewhat arbitrary. The most commonly used criterion is based on when the central maximum of one diffraction pattern falls inside the first minimum of the second pattern. The point sources are then so close that they are difficult to separate. Assuming a circular aperture for the instrument and that the angle θ_{\min} is small ($\sin \theta_{\min}; \theta_{\min}$), the resolution limit of the instrument according to the Rayleigh criterion is

$$\theta_{\min} = 1.22 \frac{\lambda}{D} \quad (3)$$

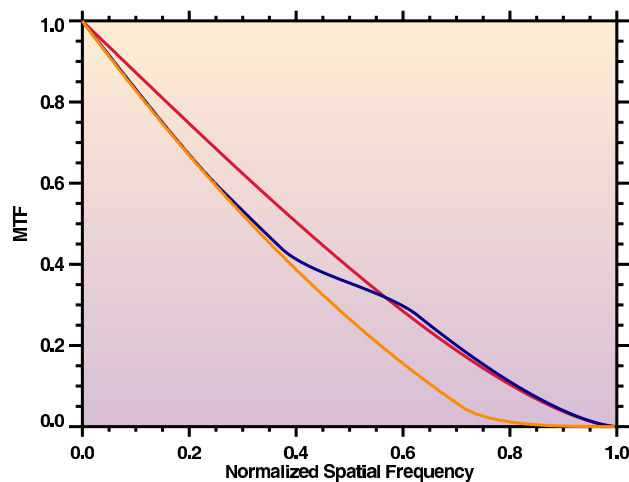


Fig. 2 Modulation transfer function. The modulation transfer function measures the ability of a system to transfer spatial information. For imaging systems with identical diffraction-limited resolution, the red curve corresponds to a circular aperture, the blue curve to a circular aperture with central obscuration, and the orange curve to a square aperture, respectively. The collecting area, however, is not the same, i.e., only 94% for the aperture with central obscuration and 64% for a square aperture as compared to their circular counterpart. Interestingly, a telescope with a square aperture and the same collecting area as a circular one can recover higher spatial frequencies due to longer baselines in the aperture function. (View this art in color at www.dekker.com.)

where θ_{\min} is expressed in radians and D is the aperture of the instrument. The ability to resolve two point sources is illustrated in Fig. 3 for the cases $\theta = 2 \cdot \theta_{\min}$ and $\theta = \theta_{\min}$ referring to clearly and barely resolved objects, respectively.

We now turn to the model of short-exposure image formation. In the following sections, we assume that the optical system can be characterized by space-invariant PSFs $S_j(x)$. We introduce here the index $j \in \{1, \dots, J\}$ enabling us to later discuss ensembles of images. A data frame $d_j(x)$ can then be expressed as the convolution of an object $f(x)$ and the PSF. In the Fourier domain we obtain, using capital letters for Fourier transforms,

$$D_j(u) = N\{F(u) \cdot S_j(u)\} \quad (4)$$

where S_j is the OTF, u is a two-dimensional spatial frequency, and $N\{\dots\}$ is a noise operator. In the Fourier domain, the complex-valued information about an image or an imaging system is arranged so that patterns that slowly vary over the field of view are close to the origin, while fine-scale information is found at higher frequencies. For brevity, we will use spatial coordinates x and frequencies u only when they are required for clarity, otherwise we omit them for the

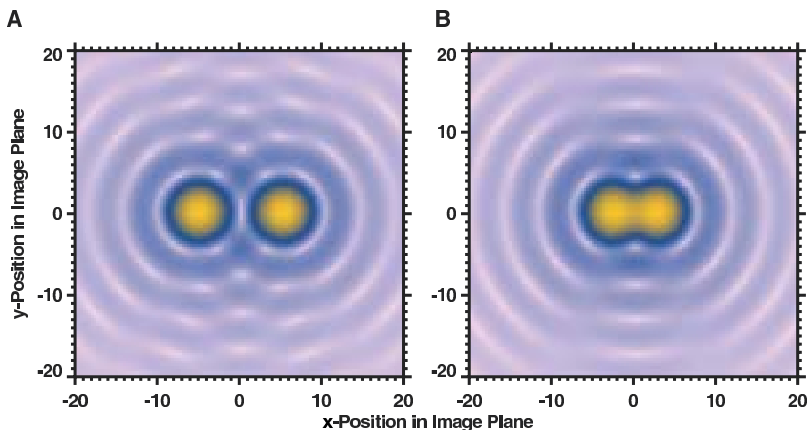


Fig. 3 Rayleigh criterion. Two point sources can be identified as distinct features if their separation is larger than $\theta_{\min} = 1.22 \cdot \lambda/D$. (A) The two point sources are well separated when $\theta = 2 \cdot \theta_{\min}$. (B) However, once approaching $\theta \cong \theta_{\min}$, the two point sources become indistinguishable. (View this art in color at www.dekker.com.)

remainder of the paper. Great simplifications can often be made if the noise operator N can be assumed to be an additive noise term with Gaussian statistics

$$D_j = F \cdot S_j + N_j \quad (5)$$

In either case, we can see that in a data frame, the information about the object and the information about the PSF are mixed. Separating this information is the goal of many image restoration methods. The PSF is determined by the pupil size and shape, and the phases across the pupil. The PSF is characterized by a generalized pupil function, which can be written as

$$P_j = A \exp\{i\phi_j\} \quad (6)$$

where ϕ_j is the instantaneous phase at the moment d_j is collected, and A is a (usually binary) function that specifies the size and shape of the pupil. The PSF can be written as

$$S_j = |F^{-1}\{P_j\}|^2 \quad (7)$$

where $F^{-1}\{\dots\}$ is the inverse Fourier transformation operator. When ϕ_j is a plane over the pupil, there are no phase aberrations and the PSF is diffraction limited, i.e., it depends only on the pupil geometry.

Speckle Imaging

Speckle imaging processes short-exposure images by estimating first the object's Fourier transform, i.e., both modulus and phase, before attempting to invert the Fourier estimate to obtain an estimate of the object itself. The term "speckle" refers to the randomly moving bright points that can be seen in the focal plane of a telescope. This speckle pattern originates from the light of a point source that took slightly different paths through the turbulent atmosphere. Each speckle represents the diffraction-limited image of the point source.

In a long-exposure image, the individual speckles are smeared out into the seeing disk, which is many times larger than the Airy disk. Even under good seeing conditions, the spatial resolution is limited to about 1 arcsec. The diffraction-limited resolution of a 1-m telescope at 600 nm is about 0.15 arcsec, i.e., the practical resolution of the telescope is about one order of magnitude worse than the resolution that could be achieved under ideal conditions without seeing.

Since the individual OTFs S_j are not known, we have to make use of average long- and short-exposure transfer functions, which are characterized by only one parameter, the Fried parameter r_0 . Roughly speaking, the Fried parameter corresponds to the aperture of the largest telescope that would just be diffraction limited. We use the spectral ratio technique to derive the Fried parameter.^[13] The spectral ratio is given by the ratio of different types of energy or power spectra

$$E = \frac{|\sum_j D_j|^2}{\sum_j |D_j|^2} = \frac{|\sum_j F|^2}{\sum_j |F|^2} \frac{|\sum_j S_j|^2}{\sum_j |S_j|^2} = \frac{|\sum_j S_j|^2}{\sum_j |S_j|^2} \quad (8)$$

Eq. (8) is independent of the object's intensity distribution and it is only a function of the two average transfer functions $|\sum_j S_j|^2$ and $\sum_j |S_j|^2$, which in turn are just functions of the Fried parameter. A closer investigation of the denominator of Eq. (8) provides insights illuminating the basic principles of speckle imaging. The second moment of the short-exposure OTFs is nonzero all the way out to the diffraction-limited cut-off frequency of the telescope.

However, we have to take an ensemble average to fill the frequency plane in the Fourier domain and thus avoiding dividing by zero. Speckle imaging is the attempt to extract unique object information from the object's energy spectrum or to use other higher moments of the short-exposure OTF to obtain diffraction-limited information. $\sum_j |S_j|^2$ is the so-called speckle transfer

function (STF). To measure the Fried parameter, the observed spectral ratios are then compared with tabulated theoretical values of the STF^[14] and the average short-exposure MTF.^[15] The amplitudes of the object's Fourier transform are then corrected according to the classical Labeyrie method,^[12] which is based on the analysis of the autocorrelation function

$$|F|^2 = \frac{\sum_j |D_j|^2}{\sum_j |S_j|^2} \quad (9)$$

To derive the phases of the object's Fourier transform, we can use the speckle masking method,^[16] which represents a certain type of triple-correlation function

$$\sum_j D_j^3(u, v) = F^3(u, v) \sum_j S_j^3(u, v) \quad (10)$$

where $D^3(u, v) = D(u)D(v)D^*(u+v)$ is the speckle masking bispectrum and ‘*’ denotes a conjugate complex quantity. $\sum_j S_j^3(u, v)$ is the average speckle masking transfer function (SMTF). The phase information, which is lost in Eq. (9), can be recovered in the triple-correlation shown in Eq. (10). Fig. 4 is an illustration of this situation comparing the auto-correlation functions of two idealized point sources in the image domain. However, a triple-correlation [Eq. (10)] as shown in Fig. 5 accesses the full phase information. In fact, the bispectrum contains several nonredundant phase relations providing reliable estimates of the object's Fourier phases. Combining real-time adaptive optics correction, frame selection and speckle masking imaging^[17] enables us to exploit the imaging capabilities of today's 1-m class solar telescopes (see Fig. 6).

Deconvolution Techniques

Deconvolution techniques require either a theoretical or a measured PSF. Theoretical PSFs can come from lens or telescope design parameters, knowledge about the movement of the object or the detector during the exposure, detector MTFs, etc. Measurements could result from an external instrument, such as a Shack-Hartmann wavefront sensor^[11] commonly used in adaptive optics, or could be derived from the image data itself (see section on Blind deconvolution). The problem is that the convolution with a PSF is a smoothing operation, which attenuates the fine details contained in the high-frequency region of the Fourier domain. Methods that attempt to undo the smoothing have to amplify the high-frequency information. At the same time, the methods have to avoid amplifying the noise, which tends to dominate at high frequencies.

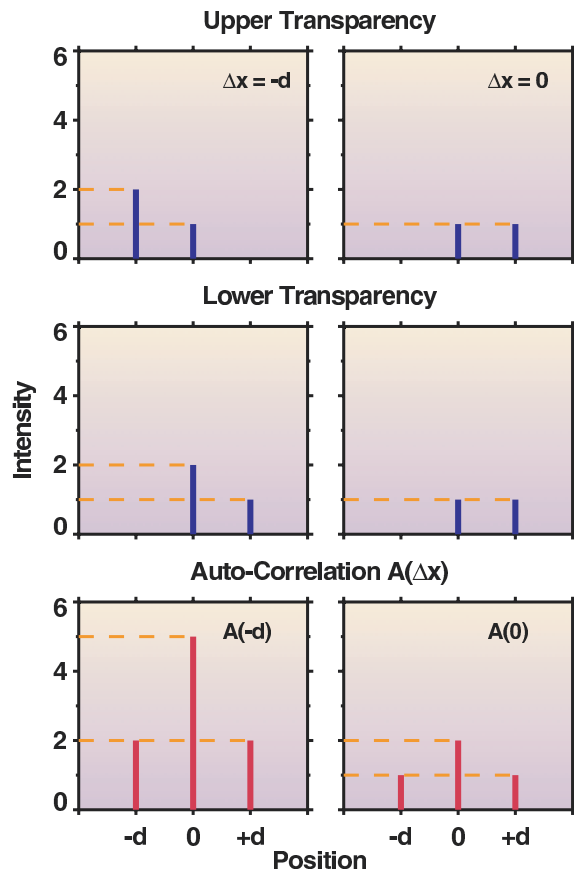


Fig. 4 Auto-correlation. The autocorrelation function of two point sources can be expressed as the convolution of their intensity distributions in the spatial domain. In an idealized approach, we can shift two transparencies across each other (the lower transparency remains in a fixed location) and obtain the autocorrelation function by adding the products of the intensity values for a certain displacement Δx . The left column shows the autocorrelation $A(\Delta x)$ of two point sources with different intensities, whereas the point sources in the right column are equally bright. Note that both functions are symmetric. We can retrieve the relative intensities and the separation of the objects. However, we cannot decide in the first case if the brighter object is to the left or right, i.e., we lost some spatial information, which is equivalent to the statement that the object's phase information is lost in the autocorrelation. (*View this art in color at www.dekker.com.*)

There are nonlinear algorithms that attempt to iteratively find an object that maximizes the likelihood that the data frame was the result of a convolution of itself and the PSF.^[18,19] The most widely used are perhaps Lucy–Richardson deconvolution,^[19,20] maximum entropy methods (MEM), and nonlinear maximum-likelihood (ML) deconvolution. For many imaging scenarios, particularly when the contrast is low and the noise is Gaussian distributed, a noniterative method, such as the Wiener filter,^[1,21] might be sufficient.^[22]

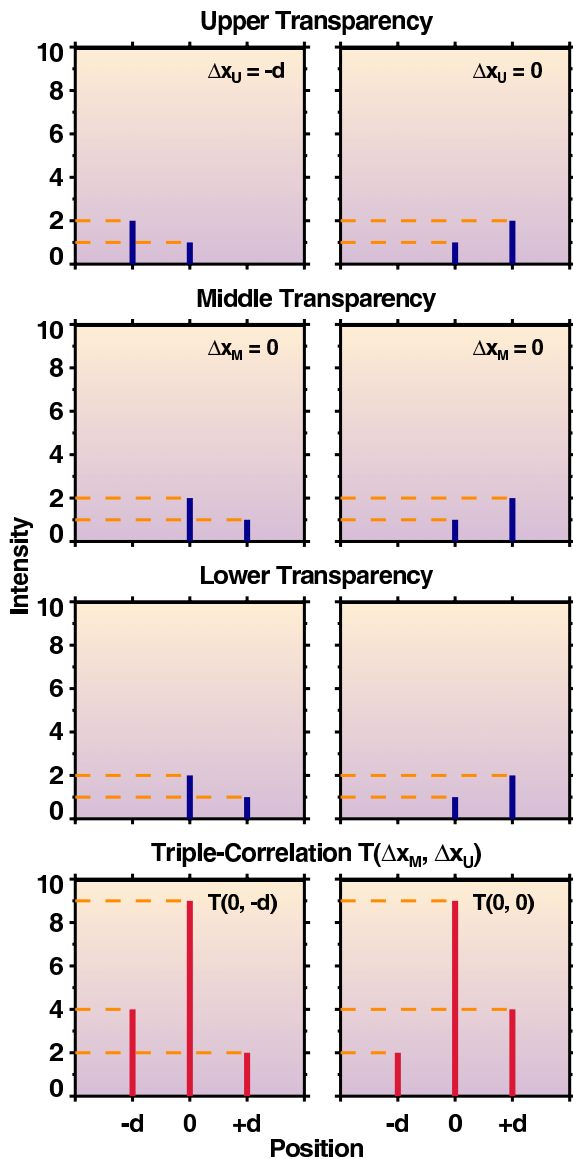


Fig. 5 Triple-correlation. We can use the same approach as for the autocorrelation function $A(\Delta x)$ to illustrate that the phase information can be retrieved in a triple-correlation $T(\Delta x_M, \Delta x_U)$. In this case, we keep the lower transparency fixed and compute the triple-correlation for a fixed displacement $T(\Delta x_M = 0, \Delta x_U)$ of the middle transparency. The asymmetry of the triple-correlation function is directly related to the object's intensity distribution and the Fourier phases. (View this art in color at www.dekker.com.)

Wiener Filter

A widely used method, and probably the simplest approach to solve the empirical restoration problem, is based on an optimum filtering process. An optimum filter is a system that uses Fourier analysis and power spectra calculations to process signals that suffer from an imperfect measurement process (e.g., smearing effects and noise). The optimum filter is based on an

explicit signal-to-noise analysis and thus differs from classical filters such as low pass, high pass and band pass filters. Optimum filters have various applications, e.g., extraction of a desired signal from a noisy measurement, signal transformation, noise suppression, separation of two signals that are mixed in one measurement, and data smoothing. The pioneering work and more formal treatment of the optimum restoration process date back to the work of Wiener in the early 1940.^[1] Optimum filters are therefore sometimes called Wiener filters. The idea behind optimum filtering is simple and can be intuitively understood if the signal-to-noise ratio (SNR) is introduced. The SNR is defined as the ratio of the signal power $P_d = |D|^2$ to the noise power $P_n = |N|^2$. Under the assumption that n is a zero-mean random processes with variance σ_n^2 , the SNR is given by the ratio of the corresponding variances σ_d^2/σ_n^2 . Consider the measured signal, e.g., an intensity distribution d as provided by Eq. (5). In the ideal case, where no noise is present in the measurement, the restoration process is trivial, as long as the degradation function S is known and exists for all spatial frequencies. Under these assumptions the simple solution to the restoration process is given by the inverse filter (Fig. 7).

$$\hat{F} = D/S = F \quad (11)$$

and the recovered spectrum \hat{F} is identical to the true object spectrum F . However, in the presence of noise, the approach

$$\hat{F} = D/S = F + N/S \quad (12)$$

will fail, because the term N/S leads to an unwanted amplification of those parts of the signal spectrum that are dominated by noise. These regions exhibit a poor SNR and give rise to artifacts in the spatial domain of the restored intensity distribution \hat{f} . Typically, these are the very high-frequency components of the spectrum that contain virtually no information about the object. We now seek to construct a real-valued function or filter W that results in the best linear estimate

$$\hat{F} = \frac{D}{S} W \quad (13)$$

of the uncorrupted object spectrum F . This should also imply that the filter 1) recovers the spectrum where the SNR is large ($\text{SNR} \gg 1$); and 2) suppresses the signal where the SNR is poor ($\text{SNR} \ll 1$). The term best linear estimate refers to the requirement that the estimate \hat{F} and the true object F should be similar. The similarity of two quantities or functions can be

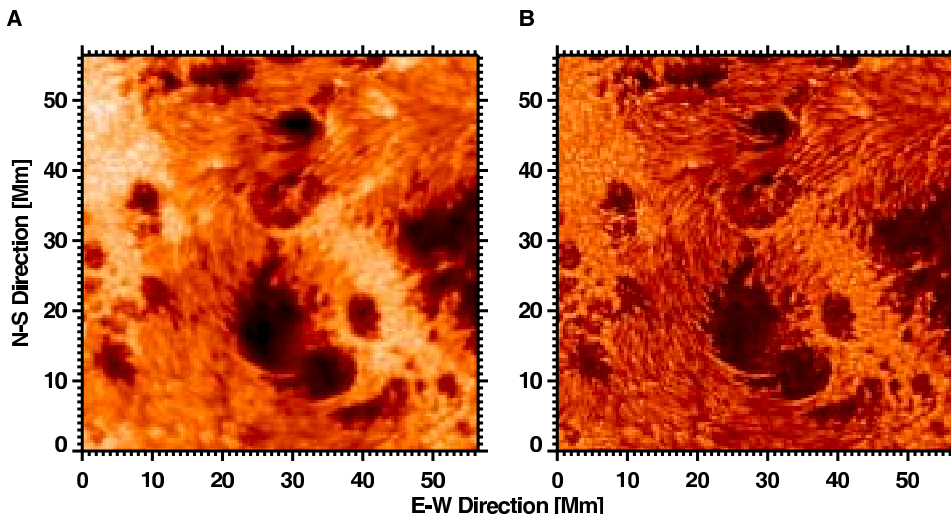


Fig. 6 Speckle masking imaging. (A) A short-exposure image is required to freeze the wavefront aberrations in an image of a solar active region, i.e., a large-scale complex of magnetic fields on the Sun. (B) Speckle masking imaging allows us to separate the object information from the wavefront distortions. Even though the input data were obtained with an adaptive optics system, it is apparent that speckle masking can achieve even higher spatial resolution approaching the diffraction limit of the telescope. The data were obtained with the Dunn Solar Telescope of the National Solar Observatory, Sacramento Peak, New Mexico. (View this art in color at www.dekker.com.)

measured by an error metric. We use the metric

$$E = \|\hat{f}(x) - f(x)\|^2 = \int |\hat{f}(x) - f(x)|^2 dx \quad (14)$$

and search for that \hat{f} that minimizes the scalar error E . Using Parseval's theorem we can transfer the minimization problem into the Fourier domain

$$E = \int |\hat{F}(u) - F(u)|^2 du = \min \quad (15)$$

Substituting Eq. (14), assuming that the signal and the noise are uncorrelated, and minimizing the integrand with respect to F , yields

$$W = \frac{|F \cdot S|^2}{|F \cdot S|^2 + |N|^2} = \frac{P_d}{P_d + P_n} \quad (16)$$

where P_d and P_n denote the power spectra of the smeared signal and the noise, respectively.

Since the optimum filter is deduced from a minimization process, errors in the filter function are of second order. Note that the filter function W does neither depend explicitly on F nor on S (which are unknowns), but only on their product $T = F \cdot S$, the noise-free degraded signal spectrum. Assuming that the power spectra almost behave additively

$$|T(u)|^2 + |N(u)|^2 \approx |D(u)|^2 \quad 0 \leq u \leq u_c \quad (17)$$

where u_c denotes the cut-off frequency, and adopting a reasonable noise model, T can be estimated or deduced directly from the observable D . If we rewrite the optimum filter function

$$W = \frac{P_d}{P_d + P_n} \sim \frac{1}{1 + SNR^{-1}} \quad (18)$$

we see that W naturally fulfills the requirements (1) and (2): The optimum filter is close to unity where the SNR

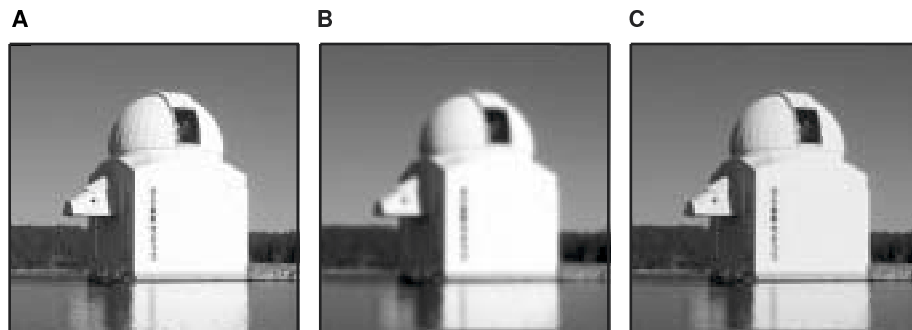


Fig. 7 Wiener filter. (A) Big Bear Solar Observatory, California. (B) The same image as in (A) but with additive Gaussian noise and subsequent convolution with an atmospheric blurring function. (C) The result of the Wiener or minimum mean-squares error filtering.

is large and close to zero where the SNR is poor and the noise dominates.

Blind Deconvolution

Without knowledge of the exact PSF, extracting the object from the convolution in Eq. (4) or (5) is a much harder problem. This problem, known as blind deconvolution (BD) is not well posed because there are infinitely many possible combinations of PSFs and objects that can make a certain image. It is necessary to use auxiliary information that constrains the solutions. One type of constraints that can be enforced is that both the object and the PSF are nonnegative and often have limited support.^[23] Another more general approach, which works for objects extending beyond the detector's field of view, is to include a model of the image formation process, and require that the PSF is physical in the sense that it corresponds to a wavefront phase over the pupil. The wavefront phase is estimated jointly with the object using a maximum-likelihood technique.^[24] The latter approach is particularly effective when several frames of the same object, but with different PSFs, are used.^[25] This is then called multiframe blind deconvolution (MFBD).

In such an MFBD algorithm, the unknown phases ϕ_j [see Eq. (6)] are expanded in suitable sets of

modes $\{\psi_m\}$

$$\phi_j = \theta_j + \sum_m \alpha_{jm} \psi_m \quad (19)$$

where θ_j can be used to represent known differences between the images (see section on Phase diversity). The ML solution corresponds to minimizing an error metric that in the general case is a function of the estimated phase expansion coefficients as well as the pixel values of the estimated object. Under the assumption of additive Gaussian noise, the metric is the least-squares difference between the data frames and the convolutions of the estimated object and the estimated PSFs. The number of unknowns can be reduced by orders of magnitude by simplifying this metric so it does not explicitly involve the object. The simplified Gaussian noise metric can be written as

$$L(\alpha) = \sum_u \left[\sum_j |D_j|^2 - \frac{|\sum_j D_j^* S_j|^2}{\gamma + \sum_j |S_j|^2} \right] \quad (20)$$

where the phase expansion coefficients enter through the OTFs and Eq. (6) and (7). The γ parameter has a noise filtering effect, much like the SNR^{-1} term in

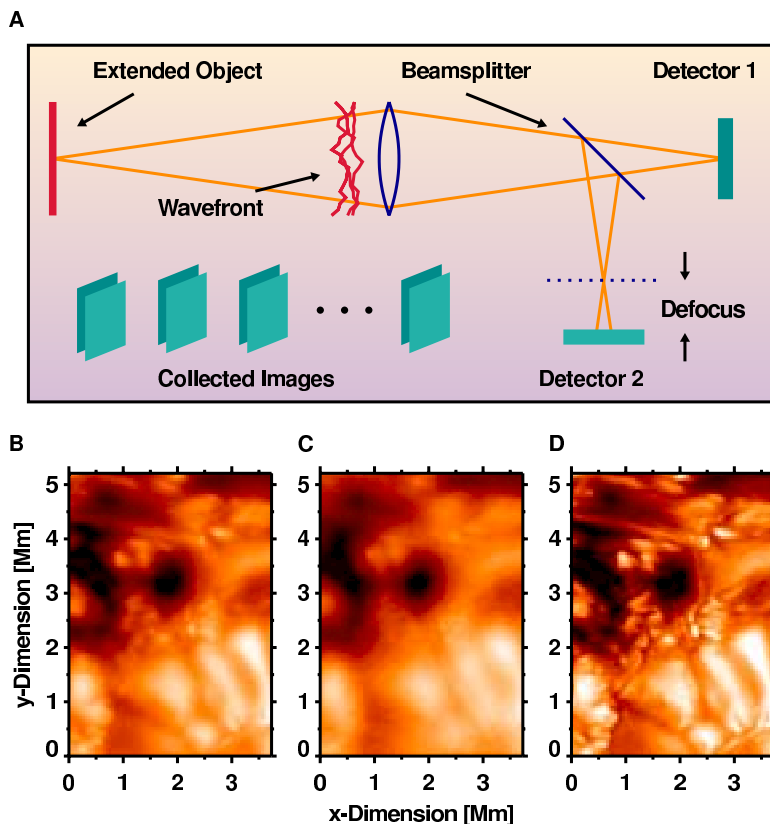


Fig. 8 Phase diversity. (A) The optical setup of a phase diversity experiment includes two detectors. One detector is located at a focus of the image forming system and an intentional focus shift has been introduced to the second detector. Pairs of (B) focal and (C) extrafocal images are acquired as input for the image reconstruction process resulting in (D) almost diffraction-limited images of solar fine structure. The dark pores and bright points in the images are signatures of strong magnetic fields on the Sun. The data were obtained with the Swedish Solar Telescope at the Observatorio del Roque de los Muchachos, La Palma, Canary Islands, Spain. (*View this art in color at www.dekker.com.*)

the simpler form of the Wiener filter (see section on Wiener Filter). The minimization of $L(\alpha)$ can then be performed by any of a number of standard optimization techniques. The data frames are then deconvolved with the PSFs estimated thus using methods similar to those described in section on Deconvolution techniques. The number of frames that are required for an adequate restoration can be less than five and still give good image quality. Results can be further improved using more frames.

Phase Diversity

Phase diversity (PD) methods^[26–29] are special cases of MFBD, where the solutions are further constrained by the particular optical setup used when collecting the data. The idea is to arrange the setup so that several images of the same object are collected, with a known difference in the wavefront phase [θ_j in Eq. (11)]. The pairs of in-focus and defocused data have to be acquired strictly simultaneously such that the wavefront distortions due to atmospheric turbulence are the same. The most commonly used phase difference is quadratic, which can be conveniently arranged by collecting intentionally defocused data along with the ordinary in-focus data (see Fig. 8). This is an improvement compared to general MFBD in two aspects: 1) The phase aberrations manifest themselves differently at different distances from the focal plane. Requiring that two PSFs result from the same phase, except for the known difference θ_j is a very strong constraint. 2) At the right distance from the focal plane (typically corresponding to a quadratic phase on the order of a wave, peak-to-peak) more information about the aberrations can be retrieved compared to the focal plane.

A single PD image pair can be sufficient for a good estimate of the phases. However, like BD, PD works better with several realizations of the atmospheric wavefront. Using more than a single pair of data frames, this method is often referred to as phase diverse speckle (PDS) imaging. The restored image in Fig. 8d is made from four pairs of in-focus and defocused images such as the ones shown in Fig. 8B and 8C, respectively. PDS generally requires a smaller number of short-exposure images than MFBD.

CONCLUSIONS

After discussing (astronomical) image restoration in some detail, we would like to conclude with a brief description of its prospects. Due to the two- and in some cases multi dimensional nature of image data sets, the data volume has been steadily increasing over the years. The next step, i.e., the collection of these

image data in centralized or federated data archives is already progressing in many specialized research disciplines. Image enhancement, pattern recognition and feature extraction will be based on restored images and only if the underlying restoration algorithms are well understood and have been proven to be reliable, we can expect to retrieve the desired image information. Context-based data searches have an enormous potential in health care and medical applications, where the detection of an abnormal pattern or the progression of a pathological pattern can be vital. In solar and space science, real-time image restoration is essential in determining the impacts of solar storms on the Sun–Earth system, which can potentially endanger space assets, human space-flight, communications technology, and the power grid. Finally, data archives become more readily accessible for a wide variety of users including researchers, educators, and the general public. Even though the access to first class research facilities might be limited, the research based on their data products and images will be open to anyone and thus leverage the investments in these facilities.

ACKNOWLEDGMENTS

This work was supported by NSF under grants ATM 03-42560, ATM 02-36945, IIS ITR 03-24816, and AST MRI 00-79482 and by NASA under grant NAG 5-12782.

REFERENCES

1. Gonzalez, R.C.; Woods, R.E. *Digital Image Processing*, 2nd Ed.; Addison-Wesley: Reading, Massachusetts, 2002.
2. Pratt, W.K. *Digital Image Processing*, 3rd Ed.; John-Wiley & Sons: New York, 2001.
3. Bracewell, R.N. *Two Dimensional Imaging*; Prentice Hall: Upper Saddle River, New Jersey, 1994.
4. Hall, E.L. *Computer Image Processing and Recognition*; Academic Press: New York, 1980.
5. IEEE Trans. Image Process. <http://www.ewh.ieee.org/soc/sps/tip/index.html>.
6. J. Opt. Soc. Am. A: Optics, Image Science and Vision, <http://josaa.osa.org/journal/josaa/about.cfm>.
7. Opt. Eng. <http://spie.org/app/Publications/index.cfm?fuseaction=journals&type=oe>.
8. Publications of the International Society of Optical Engineering (SPIE), <http://spie.org/app/Publications/>.
9. Roggemann, M.C.; Welsh, B. *Imaging Through Turbulence*; CRC Press: Boca Raton, Florida, 1996.

- 1 10. Rodier, F. *Adaptive Optics in Astronomy*;
- 2 Cambridge University Press: Cambridge, U.K,
- 3 1999.
- 4 11. Tyson, R.K. *Principles of Adaptive Optics*, 2nd
- 5 Ed.; Academic Press: San Diego, California, 1998.
- 6 12. Labeyrie, A. Attainment of diffraction limited
- 7 resolution in large telescopes by Fourier analysing
- 8 speckle patterns in star images. *Astron. Astrophys.*
- 9 **1970**, *6*, 85–87.
- 10 13. von der Lühe, O. Estimating Fried's parameter
- 11 from a time series of an arbitrary resolved object
- 12 imaged through atmospheric turbulence. *J. Opt.*
- 13 *Soc. Am. A* **1984**, *1*, 510–519.
- 14 14. Korff, D. Analysis of a method for obtaining
- 15 near-diffraction-limited information in the pre-
- 16 sence of atmospheric turbulence. *J. Opt. Soc.*
- 17 *Am.* **1973**, *63* (8), 971–980.
- 18 15. Fried, D.L. Optical resolution through a randomly
- 19 inhomogeneous medium for very long and very
- 20 short exposures. *J. Opt. Soc. Am.* **1966**, *56* (10),
- 21 1372–1379.
- 22 16. Weigelt, G. Modified astronomical speckle inter-
- 23 ferometry speckle masking." *Opt. Comm.*
- 24 **1977**, *21* (1), 55–59.
- 25 17. Denker, C.; Mascarinas, D.; Xu, Y.; Cao, W.;
- 26 Yang, G.; Wang, H.; Goode, P.R.; Rimmele, T.R.
- 27AQ1 High-spatial resolution imaging combining frame
- 28 selection, high-order adaptive optics, and speckle
- 29 masking technique. *Sol. Phys.* **2005**, *in press*.
- 30 18. Meinel, E.S. Origins of linear and non-linear
- 31 recursive restoration algorithms. *J. Opt. Soc.*
- 32 *Am. A* **1986**, *3*, 787–799.
- 33 19. Richardson, W.H. Bayesian-based iterative
- 34 method of image restoration. *J. Opt. Soc. Am.*
- 35 **1972**, *62*, 55–59.
- 36
- 37
- 38
- 39
- 40
- 41
- 42
- 43
- 44
- 45
- 46
- 47
- 48
- 49
- 50
- 51
- 52
- 53
- 54
- 55
- 56
20. Lucy, L.B. An iterative technique for the rectifi-
- cation of observed distributions. *Astron. J.*
- 1974**, *79*, 745–754.
21. Brault, J.W.; White, O.R. The analysis and
- restoration of astronomical data via the fast
- Fourier transform. *Astron. Astrophys.* **1971**, *13*,
- 169–189.
22. Fienup, J.R.; Griffith, D.; Harrington, L.;
- Kowalczyk, A.M.; Miller, J.J.; Mooney, J.A.
- Comparison of reconstruction algorithms for
- images from sparse-aperture systems. *Proc. SPIE*
- 2002**, *4792*, 1–8.
23. Ayers, G.R.; Dainty, J.C. Iterative blind deconvol-
- ution method and its application. *Opt. Lett.*
- 1988**, *13*, 547–549.
24. Holmes, T.J. Blind deconvolution of quantum-
- limited incoherent imagery. *J. Opt. Soc. Am. A*
- 1992**, *9*, 1052–1061.
25. Schulz, T.J. Multi-frame blind deconvolution of
- astronomical images. *J. Opt. Soc. Am. A* **1993**,
- 10*, 1064–1073.
26. Paxman, R.G.; Schulz, T.J.; Fienup, J.R. Joint
- estimation of object and aberrations by using
- phase diversity. *J. Opt. Soc. Am. A* **1992**,
- 9* (7), 1072–1085.
27. Gonsalves, R.A. Phase retrieval and diversity in
- adaptive optics. *Opt. Eng.* **1982**, *21* (5),
- 829–832.
28. Löfdahl, M.G.; Scharmer, G.B. Wavefront sen-
- sing and restoration from focused and defocused
- solar images. *Astrophys. J. Suppl. Ser.* **1994**,
- 107*, 243–264.
29. Löfdahl, M.G. Multi-frame blind deconvolution
- with linear equality constraints. *Proc. SPIE*
- 2002**, *4792*, 146–155.